Relative slipping at the interfaces of the flexible fiber Bragg grating sensor*

JIN Ping (金萍)[1], **WANG Yan** (王彦)[1]**, **QIN Nan** (秦楠)[1], **FANG Ting** (方挺)[1], and **WANG Haitao** (王海涛)[2]

1. *School of Electrical and Information Engineering, Anhui University of Technology, Maanshan 243000, China*
2. *The Second Construction Co., Ltd. of China Construction First Group, Beijing 100161, China*

(Received 9 February 2021; Revised 11 May 2021)

To discuss the relative slipping at the interface between a flexibly embedded fiber Bragg grating sensor and a substrate, the strain transfer was derived for an ideal case between the materials of an embedded fiber sensor. ANSYS software was used to establish a simulation model and to analyze the effects of the axial tensile force and the semi-embedded length and encapsulation substrate for the axial strain relative errors with and without relative slipping. The results of the numerical simulations show that the relative strain errors are smaller at the ends of the fibers and larger in the middle for the same tensile force, indicating that the strain transfer effect is location dependent and that the choice of a semi-embedded length of the fibers greater than 40 mm helps to reduce the relative errors. Meanwhile, five flexible sensors with different half-embedding lengths were experimentally encapsulated and subjected to axial tension-strain experiments, which showed the best strain transfer at a half-embedding length of 60 mm, and the experimental results were consistent with the numerical simulation results. The experimental results provide some theoretical and experimental basis for parameter optimization of flexible fiber grating sensors.

Document code: A **Article ID:** 1673-1905(2021)10-0604-7
DOI https://doi.org/10.1007/s11801-021-1014-5

Fiber Bragg grating (FBG) sensors have been widely used in areas such as ships, geotechnical engineering, aerospace, structural health monitoring, and offshore platforms due to their advantages of small size, small mass, anti-electromagnetic interference, high sensitivity, and resistance to corrosion[1-4]. Embedding packaging methods using flexible materials have attracted a great deal of attention[5-7].

Rocha et al[8] proposed a flexible sensor which is composed of an FBG embedded into PDMS. The experiments showed a maximum strain sensitivity of ~400 pm per 1% elongation and a resolution of ~88 pm per curvature degree. This flexible sensor also allowed high strain cycles and presented the linear behavior of ~14 pm/°C over the temperature range 20—110 °C. Niu et al[9] proposed a bent FBG embedded in PDMS to measure vertical compression load. Experiments show that the sensitivity is as high as 16.9 pm/N in the range of 0—350 N. Wang et al[10] observed that the temperature sensitivity of a silicone-based flexible sensor was 1.3 times that of a bare FBG sensor and the static pressure sensitivity was three times that of a bare FBG sensor with good repeatability. Yan et al[11] explored potential to discriminate pressure and temperature using FBGs inscribed in highly-birefringent photonic crystal fibers, the prototypes were cured in PDMS at room temperature. The FBGs embedded in the middle layer of a 2-mm-thick PDMS sheet exhibited a linear pressure sensitivity of about 2.6 pm/kPa over the range of 0—250 kPa. Park et al[12] proposed a PDMS-coated FBG temperature sensor for enhancing temperature sensitivity. By embedding the bare FBG in a temperature-sensitive elastomeric polymer, the temperature sensitivity of the proposed structure could be effectively improved by 4.2 times higher than those of the conventional bare-type FBG sensors due to the high thermal expansion coefficient of the PDMS.

When analyzing an FBG pressure sensor with the flexible embedding mentioned above, it has often been assumed that the interfaces between the substrates and intermediate layers were perfectly bonded, with no debonding and with no relative slipping or ignored asynchronous deformation between the optical fiber and the embedding material created by relative slipping under tension. However, in experiments, the bonding between a substrate and an intermediate layer is often imperfect. Considering the impacts of experimental materials, dimensions, and manufacturing process, the possible asynchronous deformation, and contact slipping that occur between a substrate and an intermediate layer should not be ignored.

* This work has been supported by the Subproject of National Key Research and Development Program of China (No.2017 YFC0805103).
** E-mail: wangyan@ahut.edu.cn

Because PDMS has good biodegradability, chemical adhesion, softness, and corrosion resistance, as well as a low elastic modulus, high resilience, and good resistance to deformation[13], PDMS was used to embed the FBG. A theoretical analysis of the strain transfer relationship between the intermediate layer and the PDMS has been performed, and an FBG substrate model with an ANSYS simulation has been built. Axial tensile testing based on the model was performed. The testing data for the case of the PDMS-FBG interface being perfectly bonded together and the testing data for the case of frictional sliding occurring between the PDMS and the FBG were compared. Ge Ziyang et al[14] analyzed the relative error of the axial strain at each point of the core caused by slip in relation to the forward pressure, but did not consider the effect of parameters such as the magnitude of the axial tension and the half-embedding length on the mean error of the axial strain calculation of the core with and without slip. The error generated when the relative slipping was ignored (the sliding friction was ignored similarly to a perfect bonding case) was calculated, namely the relative errors calculated from the fiber core axial strains obtained when relative slipping was ignored and from the fiber core axial strains obtained when relative slipping was taken into account. Then, whether the relative slipping between the substrate and FBG could be ignored has been discussed. The parameter sensitivity and factors that may have affected the relative errors were analyzed, which provide a theoretical reference for whether or not the relative slipping could be ignored, as well as the material selection for an FBG flexible pressure sensor.

The existing studies on strain transfer at the interface of embedded FBGs have assumed that the interfaces between layers in a sensor assembly are perfect (delete extra words). That is, it is assumed that the interface between the fiber and the coating layer (adhesive layer) and the interface between the coating layer (adhesive layer) and the substrate is perfectly bonded, with no relative slipping. This paper presents a PDMS-embedded FBG sensor consisting of a core, a cladding layer, a coating layer, and a PDMS. The contact slipping between the coating and the PDMS was considered. Because the grating was formed after laser writing on the optical fiber, the grating characteristics did not change much. Thus, the grating could be directly used as the fiber core for simulation calculations. The analysis model of the FBG sensor embedded in PDMS is shown in Fig.1. The optical fiber included a core and a cladding layer. In the figure, the left picture is a longitudinal view of the model, on the right is a plot of the strain transfer analysis of the substrate modulus of elasticity. Where L is the 1/2 gauge length of fiber grating, m, a, f respectively represent the variables related to the matrix, middle layer, and fiber core, r represents the radius of each layer.

Our theoretical derivation was based on the following assumptions:

(1) The mechanical properties of both the core and the cladding of the FBG were the same, and the core had only a small amount of additional Ge element compared with the cladding (the core and the cladding are hereinafter referred to as the optical fiber).

(2) The optical fiber, the coating layer, and the PDMS were isotropic linear elastic materials, and only the deformation in the axial direction of the FBG sensor was considered.

(3) The bare optical fiber and the coating layer were perfectly bonded together without relative slipping.

The focus of this study was the friction at the interface of the contacting objects. A contact could be smooth, perfectly bonded, or frictional. This study mainly examined the situation of the interface between the PDMS and the FBG under the circumstances of perfect bonding and limited friction.

For objects in contact, the contact pressure not only caused normal compression but also caused the tangential displacement of the interface. If the materials of the two objects differed, then tangential displacement was not the same, thus leading to slipping. Slipping would be resisted by friction and might be prevented to a certain extent. If the ultimate coefficient of friction was high enough, the slipping might be completely prevented.

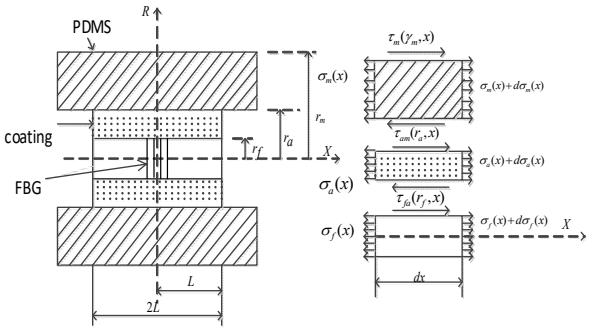

Fig.1 Analytical model of the FBG sensor in the PDMS package

Without considering the relative slip between the optical fiber and the intermediate layer, and between the intermediate layer and the substrate, Quan[15] rederived the strain transfer formula of the embedded fiber grating sensor, taking the elastic modulus of the substrate into account. The outer side of the base structure is subjected to uniform axial stress, and the micro-segment of the core is subjected to force analysis, the X-direction balance equation is:

$$\tau_{\mathrm{f,a}}(x,r_{\mathrm{f}})=\frac{1}{2\mathrm{d}x}r_{\mathrm{f}}\mathrm{d}\sigma_{\mathrm{f}}\,. \tag{1}$$

The middle segment micro-segments are

$$\tau_{\mathrm{a}}(x,r)=\frac{E_{\mathrm{f}}r_{\mathrm{f}}^2}{2r}\frac{\mathrm{d}\varepsilon}{\mathrm{d}x}\,. \tag{2}$$

The micro-sections of the matrix structure are:

$$\tau_{\mathrm{m}}(x,r)=\frac{E_{\mathrm{f}}r_{\mathrm{f}}^2}{2r}\left(1-\frac{r^2-r_{\mathrm{a}}^2}{r_{\mathrm{m}}^2-r_{\mathrm{a}}^2}\right)\frac{\mathrm{d}\varepsilon_{\mathrm{f}}}{\mathrm{d}x}\,. \tag{3}$$

Set parameters:

$$k^2=\frac{1}{\frac{1}{2}r_f^2E_f\left\{\frac{1}{G_a}\ln\frac{r_a}{r_f}+\frac{1}{G_m}\left[\frac{r_m^2}{r_m^2-r_a^2}\ln\frac{r_m}{r_a}\right]-\frac{1}{2}\right\}}. \quad (4)$$

The core and the middle layer are not directly stressed, so the ends are free end surfaces, there is no stress transmission, and the boundary conditions are:

$$\varepsilon(L, r_f)=\varepsilon(-L, r_f)=0. \quad (5)$$

The axial strain distribution in the fiber is:

$$\varepsilon_f=\varepsilon_m\left(1-\frac{\cosh(kx)}{\cosh(kL)}\right), \quad (6)$$

where m, a, f respectively represent the matrix, middle layer, and fiber core, σ indicates normal stress, τ indicates shear stress, γ represents the shear strain of each layer, r represents the radius of each layer ($r_f<r<r_a$), the X direction is the axis direction of the fiber grating sensor, E_f and E_a are the elastic modulus of the core and the middle layer respectively, ε_f, ε_a and ε_m are the axial strains of the core, middle layer, and matrix respectively, G is the shear elastic modulus of the material, and L is the 1/2 gauge length of fiber grating.

Eq.(6) shows that the axial strain of the core was affected by many factors. Assuming that the core and the cladding, the cladding and the coating layer, and the coating layer and the substrate were perfectly bonded, the axial direction of each point of the core strain was related not only to the coordinates but also to the elastic modulus of the core, the thickness and elastic modulus of the coating, the bonding length, the elastic modulus of the substrate. Unlike the ideal case, factors such as the manufacturing process in-field testing, materials, and curing time would also affect the bonding between the optical fiber coating and the substrate. When a force was applied to the substrate, the optical fiber and the substrate might slip relative to each other. When the coordinates of a point on the core changed, the axial strain at this point would also change. This study focused on whether or not relative slipping could be ignored and what factors affected it. In this study, the axial strain of the core without relative slipping was used as a baseline for comparison with the cases where relative slipping took place, and the specific effect of relative slipping on the axial strain of the core was analyzed. Because the optical fibers were embedded inside PDMS in the field-testing environment, it was difficult to observe the changes of the optical fibers and the substrate when a force was applied. Thus, the finite element simulation software ANSYS was used to simulate the strain transfer between the substrate and the optical fiber in the FBG sensor with a flexible substrate embedded under axial tension. The relative errors of the axial strain with and without relative slipping were analyzed, and the effects of the following factors on the relative errors were discussed: the embedding length, and the coefficient of friction between the coating and the substrate.

To study the relative errors of the axial strain of the optical fiber sensor embedded in a flexible substrate without slipping and with slipping after a force was applied, a finite element analysis was performed on the fiber optical sensor embedded within the PDMS. Because the model was an axisymmetric structure, only a half model was set up for the simulation analysis in this experiment. In this simulation, the optical fiber, the coating layer part, and the PDMS substrate are all selected by the sweep division method to mesh. The element size of fiber and PDMS substrate is set to 0.5 mm. The contact surface and the target surface, the edges on both ends of the fiber, and the edge where the fiber intersects with the PDMS substrate are refined. The average mesh quality is 0.870 45, with 329 415 nodes and 74 422 elements. The finite element model is shown in Fig.2.

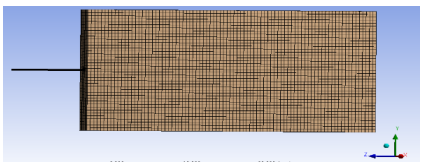

(a) PDMS meshing

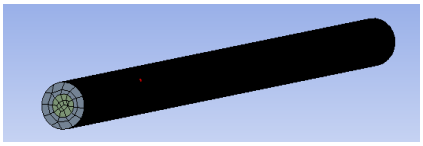

(b) Fiber meshing

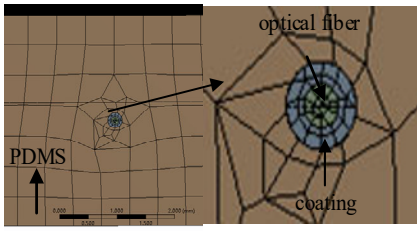

(c) Cross-section of PDMS matrix packaged fiber grating sensor

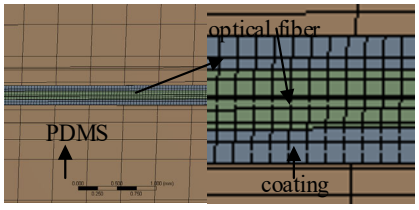

(d) Longitudinal section of PDMS matrix packaged fiber grating sensor

Fig.2 FBG fiber sensor meshing in the PDMS package

The model consisted of an optical fiber, a coating layer, and a PDMS substrate. The axial lengths of the optical fiber and the coating layer were 50 mm. The axial length of the PDMS substrate was 40 mm, which was the half-length of the optical fiber embedding. The outer diameter of the core and the cladding layer was 0.125 mm. The outer diameter of the coating layer was 0.25 mm. The length, width, and height of the cured PDMS were 40 mm, 20 mm, and 3.6 mm, respectively. The parameters of the respective layers of the materials

are shown in Tab.1.

Tab.1 Material parameters of the fiber coating and PDMS

Parameter	Value	Unit
E_f	7.2×10^{10}	Pa
E_a	2.4×10^{10}	Pa
E_m	1.2×10^{9}	Pa
μ_f	0.17	-
μ_a	0.35	-
μ_m	0.48	-
γ_f	0.062 5	mm
γ_a	0.125	mm
L	40	mm

An axial tensile force of 10 N was applied to the right end region of the PDMS. The optical fiber coating was free from force. The left end surface of the PDMS was fixed in the model set, as shown in Fig.3(a). The axial strains of the core with and without slipping were solved, as shown in Fig.3(b) and Fig.3(c). As shown in the figures, a coefficient of friction of 0.7 for the PDMS was used between 0.25 and 0.75 in this experiment.

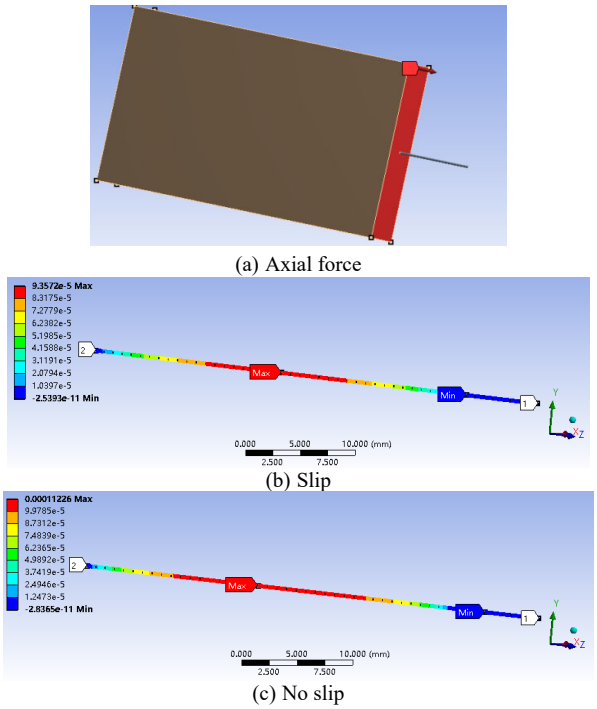

(a) Axial force

Fig.3 The axial tension of the FBG sensor in the PDMS package and the axial strain distribution of the core with or without slipping

Fig.4 shows that when the PDMS was strained under a load, the axial strain distributions of the core with and without relative slipping were essentially the same, but the axial strains corresponding to the same point were different. This showed that compared with the ideal case, in actual conditions, the changes in the shear force between the optical fiber and the PDMS may have caused relative slipping and affected the axial strain of the core. The axial strains of each point on the core central axis that were simulated with and without slipping have been compared. The relative error is the ratio of the difference between the strain and the no-skip strain. The relative errors at each point on the core central axis that resulted from ignoring the relative slipping are shown in Fig.5. It can be seen that the relative errors at the two ends of the core were relatively large, while the relative error at the middle was relatively small. This was consistent with the findings of the higher strain transfer rate in the middle region and lower strain transfer rate at both ends of the polymer-embedded optical fiber sensor.

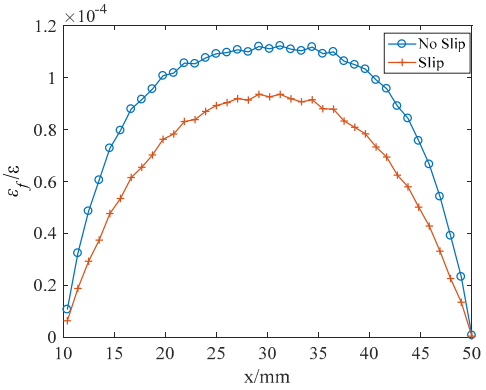

Fig.4 The axial strain corresponding to each point of the core with slipping and no slipping when the axial tensile force was 10 N

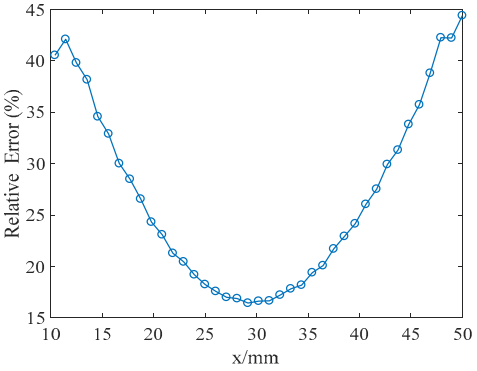

Fig.5 Relative error calculated by the core points with slipping and no slipping when the axial tensile force was 10 N

To further analyze the effect of the axial tensile force on the relative errors, an axial tensile force was incrementally applied to the PDMS from 0—10 N. The relative errors as a function of the tensile force are shown in Fig.6. It can be seen that when the tensile force was less than 1 N, the relative error increased noticeably with the increasing tensile force. When the tensile force was

between 1 N and 10 N, the relative error increased slowly. This indicated that in the range of 1—10 N, the magnitude of the tensile force had minimal effect on the relative error. The relative error reached the maximum of 24.07% for the tensile force of 10 N. The axial strain of the core was not large, the axial strains with or without slipping had the same order of magnitude, and the amount of maximum slipping was 0.000 91 mm (as shown in Fig.7). Therefore, it could be considered that for a tensile force that was less than or equal to 10 N, the relative errors could be ignored, and thus the relative slipping could be ignored.

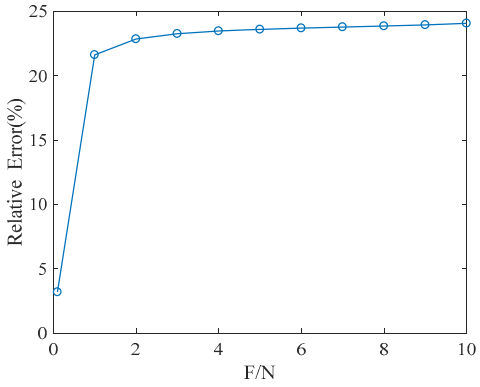

Fig.6 Relative error as a function of the tension

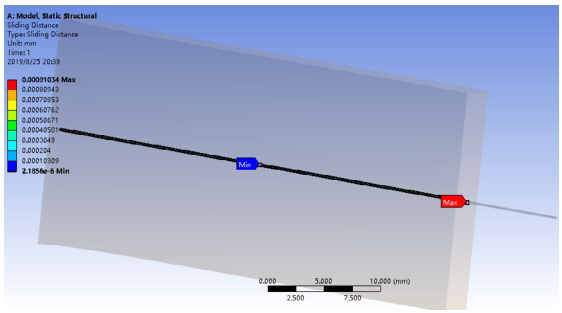

Fig.7 Relative slip distribution of each point in the core for 10 N of axial tension

In practical applications, the fiber embedded length is selected according to an actual situation. Based on Eq.(6), it could be anticipated that the above factors might have a certain effect on the axial strain of the optical fiber core, and they might affect the relative error that resulted from ignoring the relative slipping. Fig.8 shows the relationship between the relative error and the axial tensile force at different half embedding lengths. Refer to Tab.1 for other parameters. Fig.8 shows that the relative errors of different half embedding lengths varied with the axial tensile force in the same manner. From 0 N to 1 N, the relative errors increased significantly with the increasing axial tensile force. From 1 N to 10 N, the trend of increase was small. This indicated that the effect of the axial tensile force on the relative errors weakened between 1 N and 10 N. For the same axial tensile force, the relative errors gradually decreased with the increasing embedding length. Therefore, the embedding length had to be selected to be as long as possible (the half embedding length was greater than 40 mm) in an actual experiment so that the scenario could be considered as an ideal case in which the coating layer and the PDMS were bonded perfectly and there was no relative slipping as a result. For example, for an axial tensile force of 10 N, the relative error was 15.33% for the half embedding length of 60 mm.

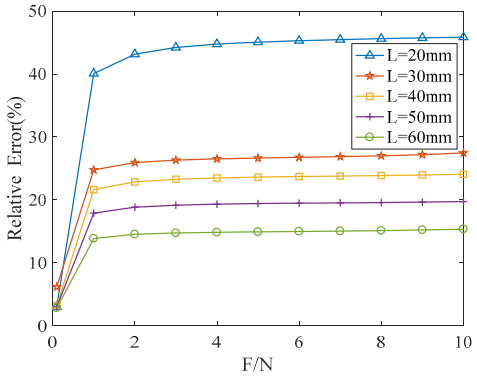

Fig.8 Relationship between the axial tensile force and the relative error for different semi-buried lengths

In practical applications, the embedded length of the optical fiber affects the strain transmission rate of the sensor, five FBG flexible sensors of different sizes are packaged to explore the strain sensitivity during axial tension. Fig.9 is the axial tensile test platform, axial tension strain tests on sensors with half-embedded lengths of 20 mm, 30 mm, 40 mm, 50 mm and 60 mm. Fig.10 shows the strain transfer rate curve of the sensor, the experimental results demonstrate that the longer the half-embedment length the higher the strain transfer efficiency, where the half-embedding length of 60 mm sensor strain transfer rate of 54.79 nm/ε, consistent with the trend of numerical simulation analysis results.

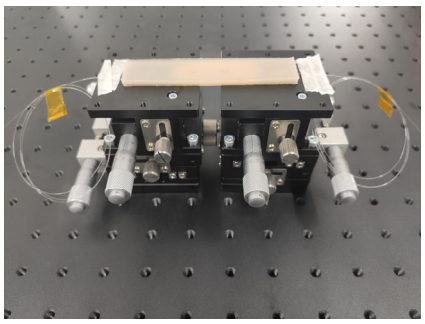

Fig.9 Axial tension test platform

The types of PDMS materials and the ratio of the mixture may have resulted in different elastic moduli for the cured substrate and different coefficients of friction for the substrate-optical fiber contact. These differences may have affected the relative errors. The coefficient of friction on human skin was mostly 0.2 to 0.5. PDMS material with coefficients of friction of 0.25

to 0.75 can be used as bionic skin, which feels like human skin and which can be very similar to human skin in structure.

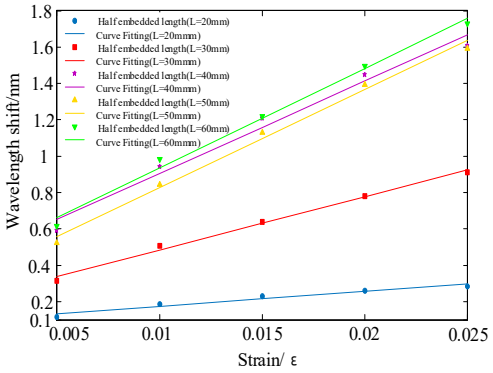

Fig.10 Transfer rate curves for sensors

Fig.11 shows the relative errors as functions of the tensile force with the elastic modulus increasing from 300 MPa to 1.5 GPa, at the coefficients of friction of 0.25, 0.5, and 0.75 in the optical fiber-subtract contact. Refer to Tab.1 for the other parameters. It can be seen that at different coefficients of friction and different elastic moduli for the PDMS, the relative errors increased with the increasing axial tensile force in the same manner. For the high elastic moduli of the PDMS, the relative errors increased rapidly from 0 N to 1 N and then increased slowly from 1 N to 10 N. For the low elastic moduli of the PDMS, the relative errors increased rapidly from 0 N to 1 N. However, between 1 N and 10 N, the relative errors were greater than those of the substrates with greater elastic moduli. It can be seen that the relative errors were small for the substrates with greater elastic moduli.

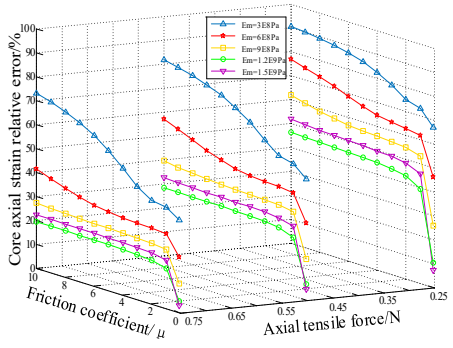

Fig.11 The relationship between the axial tensile force and the relative error of different PDMS elastic moduli when the friction coefficients were 0.25, 0.5, and 0.75

To study the effect of the coefficient of friction on the relative errors more accurately, the relationship between the elastic modulus of the PDMS and the relative error was studied for the same axial tensile force and different friction coefficients, as shown in Fig.12. Fig.12 shows that for different coefficients of friction, the relative errors decreased consistently and noticeably with the increasing elastic modulus of the PDMS. The relative errors were large for smaller coefficients of friction and smaller for larger coefficients of friction. This indicated that the larger the coefficient of friction was, the closer the actual situation was to the ideal situation and the smaller the effect of the relative slipping was. Thus, the relative slipping could be ignored. Therefore, before an experiment, the actual situation should be considered for PDMS selection. For example, in our experiment, PDMS with a coefficient of friction of 0.7 and an elastic modulus of 1.2 GPa was selected, and the relative error at an axial tensile force of 10 N was 24.07%.

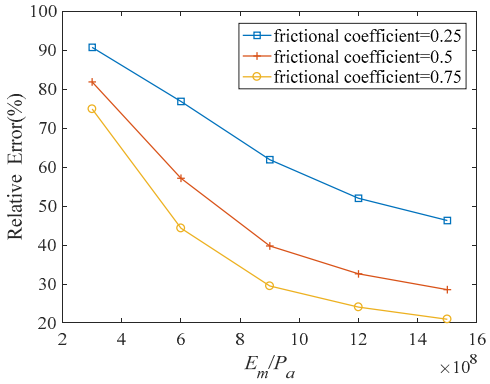

Fig.12 Relationship between the elastic modulus of the PDMS and the relative error for different friction coefficients with 10 N of axial tension

Based on the theoretical derivation of the strain transfer of the embedded polymer optical fiber sensor under ideal conditions and the established simulation model of the optical fiber FBG sensor with PDMS embedding, the effect of the axial tensile force on the relative errors that resulted from ignoring the relative slipping were analyzed. Empirical guidance was also provided for determining whether the relative slipping at the interface between the fiber and the substrate can be ignored. Furthermore, the parameters that could affect the relative errors were analyzed, which guided the material selection for an experiment. Since there have been few studies on relative slipping, this experiment may provide a reference. For optical fiber FBG sensors embedded with PDMS, the relative errors varied at various positions on the fiber under a load, and the relative errors were the smallest in the middle-section of the fiber. At a tensile force within 10 N, the maximum relative error was 24.07%. Since the relative slipping was a relatively small quantity, it could be ignored in certain cases and the actual situation could be considered an ideal situation. The parameter sensitivity analysis indicated that to ensure that relative errors were small and the relative slipping was negligible, a half embedding length of more than 40 mm needed to be adopted. In practical applications, five flexible sensors with different half-embedding lengths

were packaged for strain testing in axial tension, where the longer the embedding length, the higher the sensitivity of the sensor, The sensitivity of 54.79 nm/ε for a half-embedding length of 60 mm confirms the effect of the half-embedding length on the relative error from the side, consistent with the trend of numerical simulation analysis results. Furthermore, the substrate material had to be selected according to an actual situation.

References

[1] Floris I., Madrigal J., Sales S., Adam J. M. and Calderón P. A., Optics and Lasers in Engineering **126**, 105878 (2020).

[2] Hoffman J., Waters D. H., Khadka S. and Kumosa M. S., IEEE Transactions on Instrumentation and Measurement, **69**, 249 (2020).

[3] Bai X., Hu M., Gang T. and Tian Q., Optics and Laser Technology **112**, 467 (2019).

[4] Khan F., Denasi A., Barrera D., Madrigal J., Sales S. and Misra S., IEEE Sensors Journal **19**, 5878 (2019).

[5] Lun T. L. T., Wang K., Ho J. D. L., Lee K. H., Sze K. Y. and Kwok K. W., IEEE Robotics and Automation Letters **4**, 1454 (2019).

[6] Fajkus M, Nedoma J, Martinek R, Vasinek V and Nazeran H, Sensors **17**, 1 (2017).

[7] Rahman N, Deaton N J, Sheng J, Cheng SS and Desai JP, IEEE Robotics & Automation Letters, 1 (2019).

[8] RP Rocha, JM Gomes, JP Carmo, AF Silva and JH Correia, Optics & Laser Technology **56**, 278 (2014).

[9] Niu L., Chan C. C., Kong P. W. and Chen L. H., Bent Optical Fiber Bragg Grating Embedded in PDMS for Vertical Compression Load Sensor, Workshop on Specialty Optical Fibers and Their Applications, 2015.

[10] Wang Y., Qin N., Liu J., Liang D. and Cheng Z., Chinese Journal of Scientific Instrument **40**, 93 (2019). (in Chinese)

[11] Yan C, Ferraris E and D Reynaerts, Toward the Implementation of Flexible Sensing Sheet with Fibre Bragg Grating Sensing Elements, Proc. SPIE **8439**, 5 (2012).

[12] Chang-sub Park, Yeonjeong Han, Kyung-Il Joo, Yong Wook and Lee Shin-Won, Optics Express **18**, 24753 (2010).

[13] CS Baldwin, G Pickrell, HH Du, J Nedoma, M Fajkus, R Martinek, M Novak, O Zboril, J Jargus and K Witas, Influence of Different Encapsulation Types and Shapes of Polydimethylsiloxane on the Temperature Sensitivity of the FBG, SPIE Commercial+Scientific Sensing & Imaging, 102080U (2017).

[14] Ge Ziyang, Wang Yan, Qin Nan, Liang Dakai and Hu Xingliu, Acta Photonica Sinica **49**, 43 (2020). (in Chinese)

[15] Quan Zhiqiao, Fang Xinqiu, Xue Guangzhe, Hu Xiukun and Gu Chao, Chinese Journal of Lasers **47**, 0104004 (2020). (in Chinese)